Title

Bicuspid Aortic Valve-Associated Ascending Thoracic Aortic Aneurysm: Patient-Specific Finite Element Analysis.

Journal

The Journal of Heart Valve Disease, 24(6)

ISSN

0966-8519

Authors

Wisneski, Andrew D
Mookhoek, Aart
Chitsaz, Sam
et al.

Publication Date

2015-11-01

Peer reviewed

HHS Public Access

Author manuscript

J Heart Valve Dis. Author manuscript; available in PMC 2021 October 12.

Published in final edited form as:

J Heart Valve Dis. 2015 November ; 24(6): 714–721.

Bicuspid Aortic Valve Associated Ascending Thoracic Aortic Aneurysm: Patient-specific Finite Element Analysis

Andrew D. Wisneski, BS[1], **Aart Mookhoek, MD PhD**[2], **Sam Chitsaz, MD**[1], **Michael D. Hope, MD**[3], **Julius M. Guccione, PhD**[1], **Liang Ge, PhD**[1], **Elaine E Tseng, MD**[1]

[1]Department of Surgery, University of California San Francisco and San Francisco VA Medical Center, San Francisco, CA, USA;

[2]Department of Cardiothoracic Surgery, Erasmus University Medical Center, Rotterdam, Netherlands;

[3]Department of Radiology, University of California San Francisco and San Francisco VA.

Abstract

Background: Elective repair of bicuspid aortic valve (BAV)-associated ascending thoracic aortic aneurysms (aTAAs) is recommended at lower size limits than tricuspid aortic valve (TAV)-associated aTAAs. Rupture/dissection can occur when wall stress exceeds wall strength. We previously developed a validated computational method for determining aTAA wall stress; however, to date, this method has not applied to a patient-specific BAV aTAA. The goal of this study was to develop a patient-specific BAV aTAA computational model to determine regional wall stress, using the required zero-pressure geometry, wall thickness, material properties, and residual stress.

Methods: BAV aTAA specimen was excised intact during elective repair and zero-pressure geometry was generated using micro-computed tomography. Residual stress was determined from aTAA opening angle. ATAA material properties determined using biaxial stretch testing were incorporated into an Ogden hyperelastic model. Finite element analyses (FEA) were performed in LS-DYNA to determine wall stress distribution and magnitudes at systemic pressure.

Results: Left aTAA region had the highest stiffness, followed by the right, and then anterior/posterior walls suggesting regional variability in mechanical properties. During systole, mean principal wall stresses were 108.8kPa (circumferential) and 59.9kPa (longitudinal), while peak wall stresses were 789.4kPa (circumferential) and 618.8kPa (longitudinal). Elevated wall stress pockets were seen in anatomic left aTAA regions.

Conclusions: We developed the first to our knowledge patient-specific BAV aTAA model based upon surgical specimen. Surgical specimens serve as the gold standard for determining wall stress to validate models based on *in vivo* imaging data alone. Regions of maximal wall stress may

Corresponding Author: Elaine E. Tseng, MD, Division of Cardiothoracic Surgery, UCSF Medical Center, 500 Parnassus Ave., Suite 405W, Box 0118, San Francisco, CA, 94143-0118, USA. Phone: 415-221-4810 x3451. Fax: 415-750-2181. elaine.tseng@ucsfmedctr.org.

Presented at the American Heart Association 2013 Scientific Sessions, November 16–20, 2013, Dallas, TX.

indicate sites most prone to rupture and are crucial for evaluating rupture risk based upon the wall stress/strength relationship.

Keywords

ascending thoracic aortic aneurysm; wall stress; finite element analysis

Introduction

Elective surgical repair of ascending thoracic aortic aneurysms (aTAA) is based upon size, rate of growth, and symptoms(1). We have previously shown that a significant proportion of acute type A aortic dissections occur in patients whose aortic size did not meet size criteria for surgical intervention(2, 3), since mean aortic diameter after dissection was just under 5.0cm(3). Bicuspid aortic valve (BAV), the most common congenital cardiac abnormality, is frequently associated with aTAA(4). BAV aortic diameter increases 0.2–1.9mm/year, with lifetime rates of aortic dilatation reported in up to 59%, 78%, and 68% of BAV patients at the annulus, Sinuses of Valsalva, and sino-tubular junction (STJ), respectively(4). Mechanism for BAV aTAA is not known, but abnormal valve hemodynamics creating turbulent and asymmetric flow directed into ascending aortic wall(5) may contribute to aTAA formation(6). Furthermore, BAV aorta possesses histopathological changes of medial degeneration, with loss of vascular smooth muscle cells and fragmentation of elastic lamellae(7, 8). While BAV patients have higher rates of complications than the general population(9), comparison of aTAA complications in BAV versus tricuspid aortic valve (TAV) patients is lacking. Guidelines recommend prophylactic aTAA repair in BAV patients at smaller diameters compared to TAV patients, and recommendations for BAV aTAA repair were recently lowered to 4.5cm from 5.0cm(10). However, biomechanical data has shown that BAV aTAA has greater tensile strength in circumferential and longitudinal directions than TAV aTAA(11) which call into question the present guidelines.

Since current diameter-based guidelines are not adequate to fully capture predisposing risk factors for dissection/rupture, aTAA wall stress may serve as a more reliable predictor. Biomechanically, dissection/rupture occurs when wall stress exceeds wall strength. Unfortunately, wall stress and strength are not directly measurable *in vivo*. Use of finite element analysis (FEA) in physiologic and biomechanical studies is valuable in obtaining critical data, i.e. *in vivo* wall stress, that otherwise would be impossible to obtain. FEA of realistic 3D computational models of patient-specific aTAAs can determine wall stress, while aTAA failure testing can determine wall strength. Generalized BAV aTAA wall strength has been tested in surgical specimens(11, 12). Accurate finite element (FE) models require patient-specific 3D geometry in the zero-stress state, regional material properties, wall thickness, and residual stress. We among others have studied aTAA mechanical properties from regional stress-strain relationships(12–14). However, *in vivo* aTAA FE models(15–19) have previously been filled with assumptions that limited their accuracy and validity(20, 21). Use of *in vivo* geometry at systemic pressure from computed tomography angiography (CTA) or magnetic resonance imaging (MRI) instead of zero-stress geometry is one such assumption. *In vitro* specimens are best for obtaining zero-pressure geometry. Our prior study successfully demonstrated our methodology to create accurate (TAV)-associated

aTAA model(22). In this study, our goal was to develop the first to our knowledge BAV aTAA patient-specific FE model that accurately quantifies aortic wall stress at systemic pressure.

Materials & Methods

ATAA Mesh Generation

ATAA from 68 year-old man with BAV was excised from STJ to proximal innominate artery. Proximal and distal ends, as well as anterior, posterior, right, and left regions were noted. Informed consent was obtained for tissue use for research. Acquisition of human tissue was approved by Committee on Human Research at University of California at San Francisco Medical Center and Institutional Review Board at San Francisco Veterans Administration Medical Center.

BAV ATAA FE model was created using previously described method(22). Briefly, fresh surgical specimen underwent micro-computed tomography (microCT-40; Scanco Medical AG, Baseldorf, Switzerland) to obtain zero-pressure geometry. High resolution DICOM (Digital Imaging and Communications in Medicine) radiologic images (voxel size 76×76×76μm) were imported into ITK-SNAP (www.itksnap.org)(23). Surface mesh was formed with Rapidform XOR (INUS Technology, Inc., Sunnyvale, CA, USA). ATAA wall was filled with ~100,000 hexahedral elements (TrueGrid; XYZ Scientific, Inc., Livermore, CA, USA) to create volume mesh of accurate size and thickness at zero-stress. To determine residual stress, a thin cross-sectional ring of tissue was cut longitudinally to determine opening angle, which here was measured to be ~80degrees. ATAA residual stress was determined using a radial cut FE simulation(22). Fresh BAV aTAA specimen underwent biaxial stretch testing(13, 24). FE model was assigned material properties obtained from four anatomic regions—anterior, posterior, right, and left. Ogden hyper-elastic material, previously used to describe non-linear stress-strain relationships of arterial tissues, was chosen to model aTAA biomechanics(25). LS-DYNA (LSTC, Inc., Livermore, CA, USA) explicit FE solver was employed for pressure-loading simulations, measurement of first and second principal stresses, and lumen diameters. Maximum aTAA model diameter at systole was compared to that obtained from CTA for simulation validation.

Results

ATAA *in vivo* CT coronal slice is presented(Fig. 1). At surgery, specimen was noted to shrink in both circumferential and longitudinal directions(Fig. 2) after removal from systemic pressure. Such shrinkage exemplifies the error of utilizing *in vivo* pressurized geometry as zero-pressure state for reloading to systemic pressure during simulations. ATAA microCT images were used to create geometry and generate corresponding mesh(Fig. 3). Final unpressurized BAV aTAA geometry is shown(Fig. 4). ATAA opening angle was photographed(Fig. 5).

Stress-strain curves of aTAA regions in circumferential and longitudinal directions are shown(Fig. 6). ATAA tissue stiffness was obtained at 74kPa, corresponding to mean ascending aortic physiologic stress level under systemic pressure. Ascending aortic stress

level was calculated based upon Laplace equation considering mean systemic pressure of 100mmHg and using average aortic thickness and diameter. ATAA stiffness at 74kPa in circumferential direction was highest in the left region (1238.7kPa), followed by anterior (615.6kPa), right (608.2kPa) and posterior (316.1kPa). ATAA stiffness at 74kPa in longitudinal direction was greatest in the left region (1269.5kPa), followed by right (667.8kPa), anterior (617.9kPa), and posterior (423.8kPa). No significant differences in stiffness between circumferential and longitudinal directions in each region were noted so aTAA was modeled as isotropic.

At systole, peak aTAA first principal wall stress (FPS) primarily in circumferential direction was 789.4kPa with mean 108.8kPa(Fig. 7). Peak aTAA second principal wall stress (SPS) primarily in longitudinal direction was 618.8kPa with mean 59.9kPa. At diastole, peak FPS was 651.3kPa with mean 72.2kPa; while peak SPS was 495.6kPa with mean 37.9kPa. Difference in peak FPS was 138.1kPa throughout the cardiac cycle, while that for peak SPS was 123.2kPa. Difference in mean FPS throughout the cardiac cycle was 36.6kPa, while that for mean SPS was 22kPa. Maximum diameter of the proximal lumen ranged 51.5 to 53.1mm from diastole to systole, while distal lumen ranged 37.6 to 39.2mm. ATAA distensibility, the change in diameter from diastole to systole, at systole was 3.1% proximally and 4.2% distally. A pocket of maximal wall stress, could be appreciated at anatomical left region(Fig. 8). Excellent diameter correlation was exhibited when comparing model in systole to pre-operative CTA.

Discussion

Dissection/rupture of ascending thoracic aortic aneurysms (aTAA) are catastrophic, often lethal cardiovascular emergencies. Ideally, criteria to determine patient-specific risk of dissection/rupture would be established. Surgical risks would only be incurred for small aTAA patients at increased risk. We developed the first to our knowledge validated FE model of a patient-specific BAV aTAA using surgical specimen to determine wall stress distribution and magnitude at systemic pressure. Unlike previously created models(15–19), BAV patient’s surgical aTAA was used to obtain zero-stress geometry, unloaded wall thickness, regional material properties, and residual stress.

Patient-Specific Regional Material Properties

We previously characterized BAV and TAV aTAA mechanical properties(13). No obvious differences in anterior and posterior aTAA regional mechanical properties were seen; but, right and left regions were not studied. Similarly, stress-strain curves in anterior and posterior regions of this patient were nearly superimposed; however, significant differences were seen in the left compared to right, anterior, and posterior regions. Left aTAA region had greatest stiffness than other regions. While further study of regional aTAA mechanical properties incorporating right and left regions will be necessary, this patient-specific aTAA suggests regional material differences exist and that computational models incorporating average literature-based aTAA material properties uniformly applied may not yield realistic physiologic results.

aTAA Distensibility and Wall Stress

Minimal distensibility (3–4%) was seen proximally and distally, with diameter changes of only 1.6mm from diastole to systole at systemic pressure. Normal aortic distensibility is age dependent with 10±3% circumferential distensibility in younger patients vs. 3±1% in older patients(26). This patient's aTAA distensibility was within expected range for elderly patients without aTAA or BAV. Mean aTAA FPS from diastole to systole at systemic pressure (72.2–108.8kPa), was within peak stress range seen in normal aortic root(27). Peak aTAA FPS in systole was ~7x greater than mean wall stress. Peak wall stress ranged from 651.3–789.4kPa circumferentially and 495.6–618.8kPa longitudinally from diastole to systole at systemic pressure. Peak wall stress distribution was concentrated in left aTAA region proximally and near STJ. Dissection/rupture could occur in this region in the absence of surgical repair.

Wall Strength

Pham et al. determined BAV aTAA wall strength using uniaxial failure testing in 20 patients with mean diameter of 5.01cm and mean age of 55(12). One limitation was that samples were cryopreserved prior to mechanical testing; the impact of freezing on changes in wall strength is unknown. Circumferential BAV aTAA wall strength was ~2200kPa, similar to that of longitudinal wall strength of ~2100kPa. In contrast, Pichamuthu et al. found aTAA was stronger circumferentially than longitudinally in 23 BAV aTAA patients with average age 54 and mean aTAA diameter 5cm. These samples were stored at 4°C and tested within 48 hours of harvesting. BAV aTAA tensile strength was 1656±980kPa circumferentially and 698±310kPa longitudinally. Our patient's aTAA would not have predicted to rupture circumferentially based on the range of his peak aTAA FPS. On the other hand, his peak SPS were within range of BAV aTAA longitudinal failure strength, suggesting that his aTAA could yield longitudinally at higher blood pressures creating a circumferential tear predisposing to aortic dissection. Our patient-specific FE model served to validate the need for surgical intervention in this patient and predict a possible failure mechanism.

Comparison to TAV aTAA Model

We recently published a patient-specific FE model of TAV aTAA(22). Comparing regional tissue stiffness at 74kPa, both anatomic left regions of TAV and BAV aTAAs experience the greatest stiffness compared to other regions. Stiffness values of TAV aTAA left proximal and distal regions were 1420.88kPa and 1375.11kPa (circumferential), respectively, and 1410.2kPa and 1364.11kPa (longitudinal), respectively. BAV aTAA patient presented here did not have separate proximal and distal material property data, but BAV left regional tissue stiffness (1238.7kPa circumferential, 1269.5kPa longitudinal) had similar magnitude to that of TAV aTAA. Why left regional stiffness is greatest in magnitude is unknown, but apposition to the pulmonary artery may be a contributor. Interestingly, throughout the cardiac cycle, TAV aTAA distensibility, 5–6%, was greater than that of BAV aTAA, 3–4%, despite greater TAV stiffness.

Comparing stresses, this BAV aTAA patient had greater peak FPS and SPS (789.4kPa and 618.8kPa, respectively) than those of the prior TAV aTAA patient (545.1kPa and 430.1kPa, respectively). In contrast, TAV aTAA had greater mean FPS and SPS (172.0kPa

and 71.9kPa, respectively) compared to BAV aTAA stresses (108.8kPa and 59.9kPa, respectively). Greater peak FPS and SPS in BAV aTAA suggests a localized region experiencing extremely high stress compared to the rest of the aneurysm. Greater mean FPS and SPS of TAV aTAA suggests that the regions of high stress are of greater area within the aneurysm. This observation was corroborated by examining the stress models where BAV aTAA has a distinct region of peak stress in the left proximal aneurysm whilst TAV aTAA has areas of stress more widespread throughout the left and right regions. Regional geometry and material properties of BAV aTAA likely contribute to such a distinct region of elevated wall stress. TAV aTAA also experienced greater difference in peak FPS from diastole to systole (197.9kPa) compared to that of BAV 138.1kPa.

ATAA Computational Models

While not directly comparable with our study, Nathan et al. examined ascending aortic wall stress in BAV patients using FEA. Models were created based upon pressurized CTA geometry, wall thickness from trans-thoracic echocardiography, and literature-based material properties(16). Average BAV patient age was significantly younger (49 years) than our patient (68 years) where age significantly impacts mechanical properties and stiffness. Furthermore, BAV aTAA size averaged 4.0cm, much smaller than our patient. In contrast to peak wall stress, they reported 99th percentile wall stress which was 540±60kPa in BAV patients. While similar in wall stress magnitude to our patient, the influence of altering their simulations to reflect our patient's older age, larger diameter, and nonuniform material properties makes direct comparison not possible. In their study, location of 99th percentile wall stress in BAV, occurred in ascending aortic convexity in anatomic left region (50%) and in concavity of anatomic right (45%). In our BAV aTAA patient, peak aneurysm wall stress was located in the anatomic left region.

Computational fluid dynamics (CFD) or fluid-structure interaction (FSI) simulations have been performed to study how hemodynamic factors such as flow patterns and wall shear stress could lead to aTAA development and growth. Using CFD, Viscardi et al. studied how differences in BAV and TAV hemodynamics impact wall shear stress(19). Peak systolic jet velocities were nearly two-fold greater (5.0m/s) for BAV than TAV (2.3m/s). BAV flows were more asymmetric, had more pronounced recirculation zones and eddy currents within ascending aorta, and had flow velocity directed toward mid-ascending aorta convexity. Using FSI, Pasta et al. demonstrated that sites of maximum wall shear stress occurred in anterolateral ascending aorta suggesting this region was susceptible to aTAA development and enlargement(18). BAV aTAA exhibited left-handed nested helical flow in ascending aorta similar to that shown by our group(5).

Future Model Development

Development of further patient-specific models based on surgical specimens will enable us to better understand differences between TAV and BAV wall stress magnitude, distribution, and their contribution to dissection/rupture. Currently, surgical patients undergoing elective repair are identified as high risk for rupture/dissection based upon size. Patient-specific FE aTAA models in surgical patients can yield a range of wall stresses reflecting new thresholds for elective repair in relation to failure strength. Demonstrating peak wall stresses

fall within range of aTAA failure strength (as shown in this study), could allow application of wall stress magnitude thresholds to smaller aneurysms which despite their size may reach critical stress values. Furthermore, these models can determine whether the clinical practice of earlier operation on BAV aTAA is justified biomechanically. These models based upon experimentally obtained parameters from surgical specimens serve as the gold-standard by which to compare corresponding models derived from *in vivo* data.

Patient-specific aTAA FE models based solely on *in-vivo* parameters require validation to be reliable for clinical use. Model geometry obtained from *in vivo* imaging reflects hemodynamic loading forces, not zero-stress state, which could be obtained by inverse FE modeling to effectively shrink aTAA geometry to unloaded state. Wall thickness and regional material properties cannot be determined by CTA but may be estimated *in vivo* using Cine Displacement Encoding with Simulated Echos (DENSE)-MRI. We recently performed the first computational aTAA models derived from *in-vivo* imaging while accounting for zero-pressure geometry and patient specific material properties(28). Patient-specific aTAA computational models were created from *in-vivo* ECG-gated CTA and DENSE-MRI. We found that peak FPS aTAA stress was 430.6kPa and peak SPS was 200.7kPa in systole. Without zero-pressure correction, FEA results significantly underestimated peak FPS and SPS (312.5kPa and 156.2kPa, respectively). The importance of zero-pressure geometry was demonstrated in these models to attain accurate results. Peak FPS and SPS results were lower than those of the BAV aTAA patient above, but those models were of <5.0cm aTAAs.

Study Limitations

While we successfully identified differences in tissue stiffness and material properties within defined anatomic regions, we assumed that within those regions, aTAA was homogeneous. More pronounced regional variations could exist, but we incorporated regional differences to a greater degree than previous models. Our data from circumferential versus longitudinal stress-strain curves had no significant differences, which correlates with data of Pham et al(12). As such, this patient's aTAA tissue was isotropic. Lastly, our simulation did not account for FSI or asymmetric or turbulent flow patterns from the valve. ATAA dissection/rupture depends upon understanding wall stress, and wall stress based on pressure (FEA) is of significantly greater magnitude than the contribution of fluid shear stress whose maximum value was estimated to be 0.0023kPa(18) by FSI. It is possible, however that aTAA development and growth could depend on eccentricities of flow and FSI may be important for predicting growth. Unlike FEA that requires surgical specimens for accuracy, FSI studies require accurate flow input conditions which can be obtained *in vivo* noninvasively by 4D-flow MRI. Such investigation was beyond the scope of this work.

Conclusions

We report the first to our knowledge of a patient-specific BAV aTAA FE model developed from an intact freshly excised surgical specimen that incorporated zero-pressure geometry, wall thicknesses, residual stress, and regional material properties. Mean wall stress was within range of normal peak wall stress for ascending aorta; however, peak wall stress

was significantly less than reported circumferential BAV aTAA strength but within limits of longitudinal BAV aTAA strength. Peak wall stress was identified in this patient in left anatomic region just above STJ. Our data suggests that risk of longitudinal failure with a circumferential tear could be a possible predisposing mechanism for dissection in the absence of surgical repair. Creation of such accurate FE models based on surgical specimens is a vital first step in the development of biomechanically based clinical paradigm for *in-vivo* patient-specific aTAA risk prediction(22).

REFERENCES

1. Elefteriades JA. Indications for aortic replacement. The Journal of thoracic and cardiovascular surgery. 2010;140(6 Suppl):S5–9; discussion S45–51. Epub 2010/12/01. [PubMed: 21092797]
2. Pape LA, Tsai TT, Isselbacher EM, Oh JK, O'Gara PT, Evangelista A, et al. Aortic diameter >or = 5.5 cm is not a good predictor of type A aortic dissection: observations from the International Registry of Acute Aortic Dissection (IRAD). Circulation. 2007;116(10):1120–7. Epub 2007/08/22. [PubMed: 17709637]
3. Jaussaud N, Chitsaz S, Meadows A, Wintermark M, Cambronero N, Azadani AN, et al. Acute type A aortic dissection intimal tears by 64-slice computed tomography: a role for endovascular stentgrafting? J Cardiovasc Surg (Torino). 2013;54(3):373–81. Epub 2012/07/24.
4. Tadros TM, Klein MD, Shapira OM. Ascending aortic dilatation associated with bicuspid aortic valve: pathophysiology, molecular biology, and clinical implications. Circulation. 2009;119(6):880–90. Epub 2009/02/18. [PubMed: 19221231]
5. Hope MD, Wrenn J, Sigovan M, Foster E, Tseng EE, Saloner D. Imaging biomarkers of aortic disease: increased growth rates with eccentric systolic flow. J Am Coll Cardiol. 2012;60(4):356–7. Epub 2012/07/21. [PubMed: 22813616]
6. Burris NS, Sigovan M, Knauer HA, Tseng EE, Saloner D, Hope MD. Systolic Flow Displacement Correlates With Future Ascending Aortic Growth in Patients With Bicuspid Aortic Valves Undergoing Magnetic Resonance Surveillance. Invest Radiol. 2014. Epub 2014/05/03.
7. Nataatmadja M, West M, West J, Summers K, Walker P, Nagata M, et al. Abnormal extracellular matrix protein transport associated with increased apoptosis of vascular smooth muscle cells in marfan syndrome and bicuspid aortic valve thoracic aortic aneurysm. Circulation. 2003;108 Suppl 1:Ii329–34. Epub 2003/09/13. [PubMed: 12970255]
8. de Sa M, Moshkovitz Y, Butany J, David TE. Histologic abnormalities of the ascending aorta and pulmonary trunk in patients with bicuspid aortic valve disease: clinical relevance to the ross procedure. The Journal of thoracic and cardiovascular surgery. 1999;118(4):588–94. Epub 1999/10/03. [PubMed: 10504620]
9. Michelena HI, Khanna AD, Mahoney D, Margaryan E, Topilsky Y, Suri RM, et al. Incidence of aortic complications in patients with bicuspid aortic valves. JAMA : the journal of the American Medical Association. 2011;306(10):1104–12. Epub 2011/09/16. [PubMed: 21917581]
10. Hiratzka LF, Bakris GL, Beckman JA, Bersin RM, Carr VF, Casey DE Jr., et al. 2010 ACCF/AHA/AATS/ACR/ASA/SCA/SCAI/SIR/STS/SVM Guidelines for the diagnosis and management of patients with thoracic aortic disease. A Report of the American College of Cardiology Foundation/American Heart Association Task Force on Practice Guidelines, American Association for Thoracic Surgery, American College of Radiology,American Stroke Association, Society of Cardiovascular Anesthesiologists, Society for Cardiovascular Angiography and Interventions, Society of Interventional Radiology, Society of Thoracic Surgeons,and Society for Vascular Medicine. J Am Coll Cardiol. 2010;55(14):e27–e129. Epub 2010/04/03. [PubMed: 20359588]
11. Pichamuthu JE, Phillippi JA, Cleary DA, Chew DW, Hempel J, Vorp DA, et al. Differential Tensile Strength and Collagen Composition in Ascending Aortic Aneurysms by Aortic Valve Phenotype. Ann Thorac Surg. 2013. Epub 2013/09/12.
12. Pham T, Martin C, Elefteriades J, Sun W. Biomechanical characterization of ascending aortic aneurysm with concomitant bicuspid aortic valve and bovine aortic arch. Acta Biomater. 2013;9(8):7927–36. Epub 2013/05/07. [PubMed: 23643809]

13. Azadani AN, Chitsaz S, Mannion A, Mookhoek A, Wisneski A, Guccione JM, et al. Biomechanical properties of human ascending thoracic aortic aneurysms. Ann Thorac Surg. 2013;96(1):50–8. Epub 2013/06/05. [PubMed: 23731613]

14. Okamoto RJ, Xu H, Kouchoukos NT, Moon MR, Sundt TM 3rd. The influence of mechanical properties on wall stress and distensibility of the dilated ascending aorta. J Thorac Cardiovasc Surg. 2003;126(3):842–50. Epub 2003/09/23. [PubMed: 14502164]

15. Beller CJ, Labrosse MR, Thubrikar MJ, Robicsek F. Role of aortic root motion in the pathogenesis of aortic dissection. Circulation. 2004;109(6):763–9. Epub 2004/02/19. [PubMed: 14970113]

16. Nathan DP, Xu C, Plappert T, Desjardins B, Gorman JH 3rd, Bavaria JE, et al. Increased ascending aortic wall stress in patients with bicuspid aortic valves. Ann Thorac Surg. 2011;92(4):1384–9. Epub 2011/08/27. [PubMed: 21867987]

17. Thubrikar MJ, Agali P, Robicsek F. Wall stress as a possible mechanism for the development of transverse intimal tears in aortic dissections. J Med Eng Technol. 1999;23(4):127–34. Epub 1999/11/24. [PubMed: 10561823]

18. Pasta S, Rinaudo A, Luca A, Pilato M, Scardulla C, Gleason TG, et al. Difference in hemodynamic and wall stress of ascending thoracic aortic aneurysms with bicuspid and tricuspid aortic valve. J Biomech. 2013;46(10):1729–38. Epub 2013/05/15. [PubMed: 23664314]

19. Viscardi F, Vergara C, Antiga L, Merelli S, Veneziani A, Puppini G, et al. Comparative finite element model analysis of ascending aortic flow in bicuspid and tricuspid aortic valve. Artif Organs. 2010;34(12):1114–20. Epub 2010/07/14. [PubMed: 20618222]

20. Georgakarakos E, Ioannou CV, Papaharilaou Y, Kostas T, Katsamouris AN. Computational evaluation of aortic aneurysm rupture risk: what have we learned so far? J Endovasc Ther. 2011;18(2):214–25. Epub 2011/04/28. [PubMed: 21521062]

21. Reeps C, Gee M, Maier A, Gurdan M, Eckstein HH, Wall WA. The impact of model assumptions on results of computational mechanics in abdominal aortic aneurysm. J Vasc Surg. 2010;51(3):679–88. Epub 2010/03/09. [PubMed: 20206812]

22. Wisneski AD, Mookhoek A, Chitsaz S, Hope MD, Guccione JM, Ge L, et al. Patient-specific finite element analysis of ascending thoracic aortic aneurysm. Journal of Heart Valve Disease. 2014;23(6):765–72.

23. Yushkevich PA, Piven J, Hazlett HC, Smith RG, Ho S, Gee JC, et al. User-guided 3D active contour segmentation of anatomical structures: significantly improved efficiency and reliability. Neuroimage. 2006;31(3):1116–28. Epub 2006/03/21. [PubMed: 16545965]

24. Azadani AN, Chitsaz S, Matthews PB, Jaussaud N, Leung J, Tsinman T, et al. Comparison of mechanical properties of human ascending aorta and aortic sinuses. Ann Thorac Surg. 2012;93(1):87–94. Epub 2011/11/15. [PubMed: 22075218]

25. Holzapfel GA, Ogden RW. Modelling the layer-specific three-dimensional residual stresses in arteries, with an application to the human aorta. J R Soc Interface. 2010;7(46):787–99. Epub 2009/10/16. [PubMed: 19828496]

26. Morrison TM, Choi G, Zarins CK, Taylor CA. Circumferential and longitudinal cyclic strain of the human thoracic aorta: age-related changes. J Vasc Surg. 2009;49(4):1029–36. Epub 2009/04/04. [PubMed: 19341890]

27. Grande KJ, Cochran RP, Reinhall PG, Kunzelman KS. Stress variations in the human aortic root and valve: the role of anatomic asymmetry. Ann Biomed Eng. 1998;26(4):534–45. Epub 1998/07/14. [PubMed: 9662146]

28. Krishnan KGL, Haraldsson H, Hope MD, Saloner DA, Guccione JM, Tseng EE. Ascending Thoracic Aortic Aneurysm Wall Stress Analysis Using Patient-Specific Finite Element Modeling of in vivo Magnetic Resonance Imaging. Interact Cardiovasc Thorac Surg. 2015, in press.

Figure 1:
Coronal slice from aTAA ECG-gated CTA.

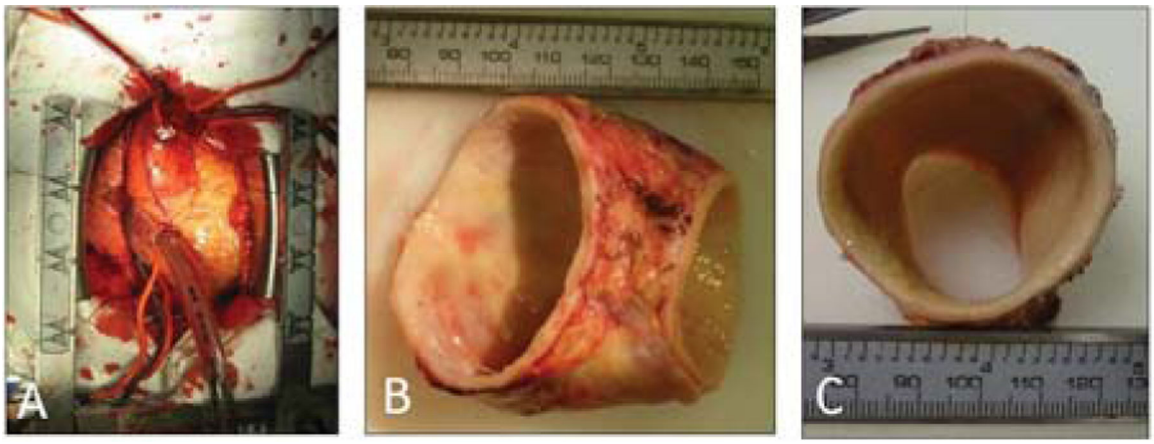

Figure 2:
ATAA: a) at surgery prior to excision, b) excised posterior view, 2c) en face.

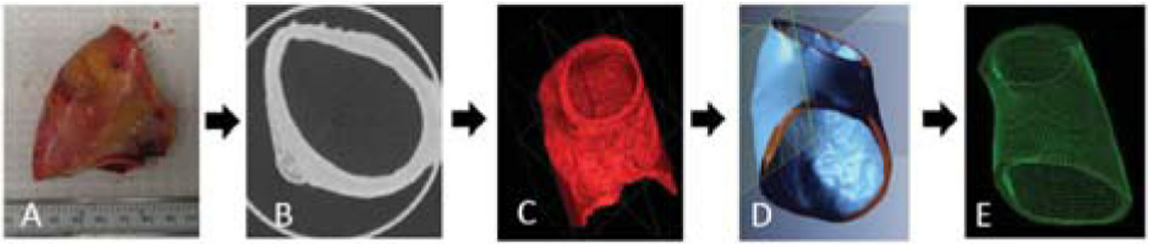

Figure 3:
Model generation: 3a) Excised aTAA (side view), 3b) Axial slice from microCT, 3c) Segmentation with ITK-Snap, 3d) Surfaces smoothed with RapidForm, 3e) Mesh generation with TrueGrid.

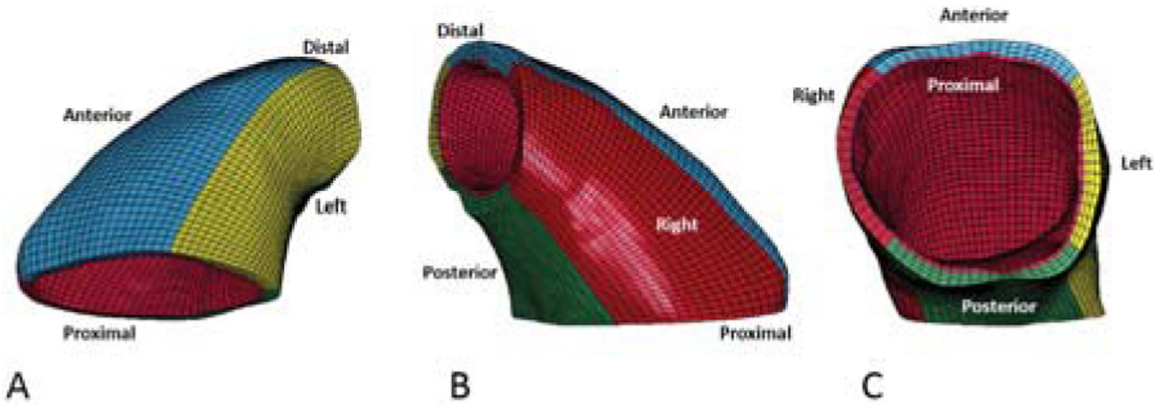

Figure 4:
BAV aTAA model (3 views) with unpressurized, zero-stress geometry.

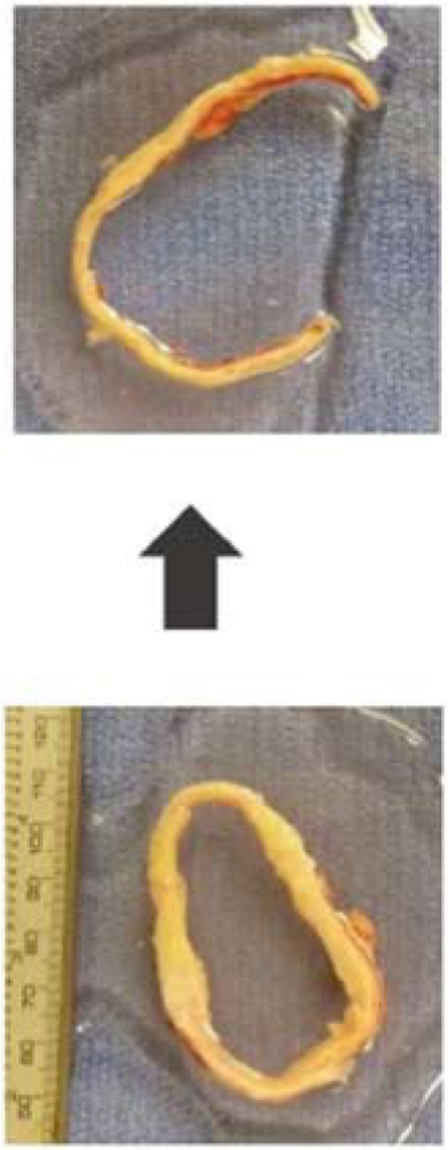

Figure 5:
ATAA opening angle.

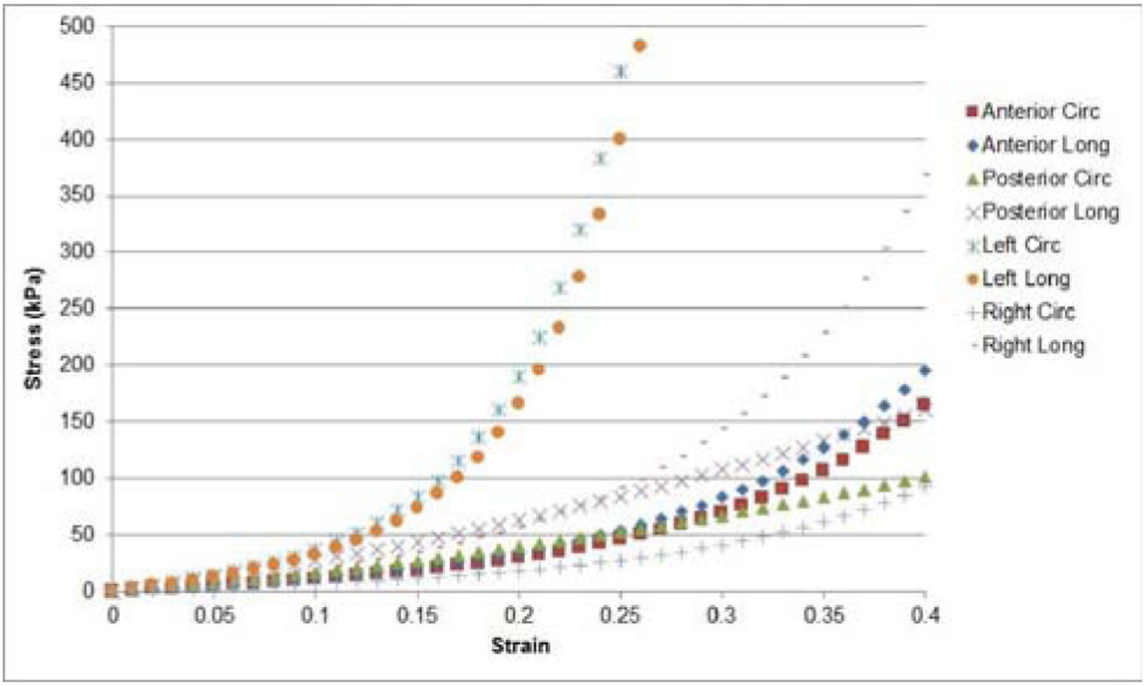

Figure 6:
Circumferential and longitudinal stress-strain curves of aTAA specimen.

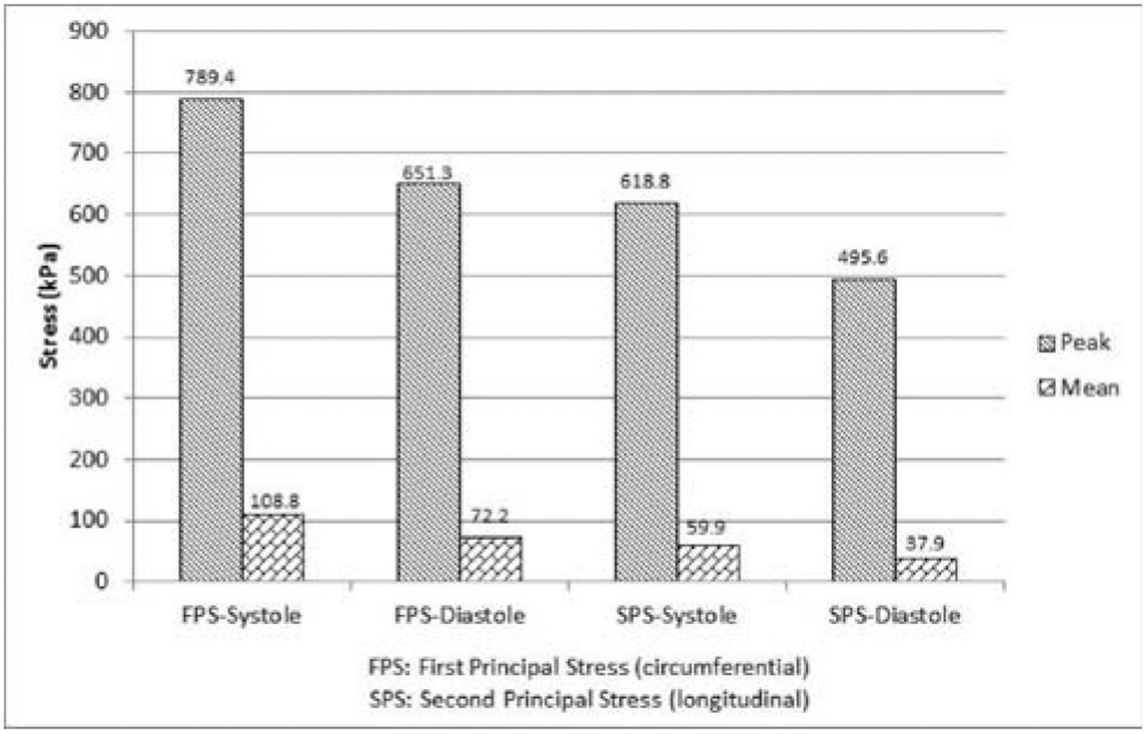

Figure 7:
First and second principal wall stresses (FPS and SPS, respectively) in diastole and systole at systemic pressure.

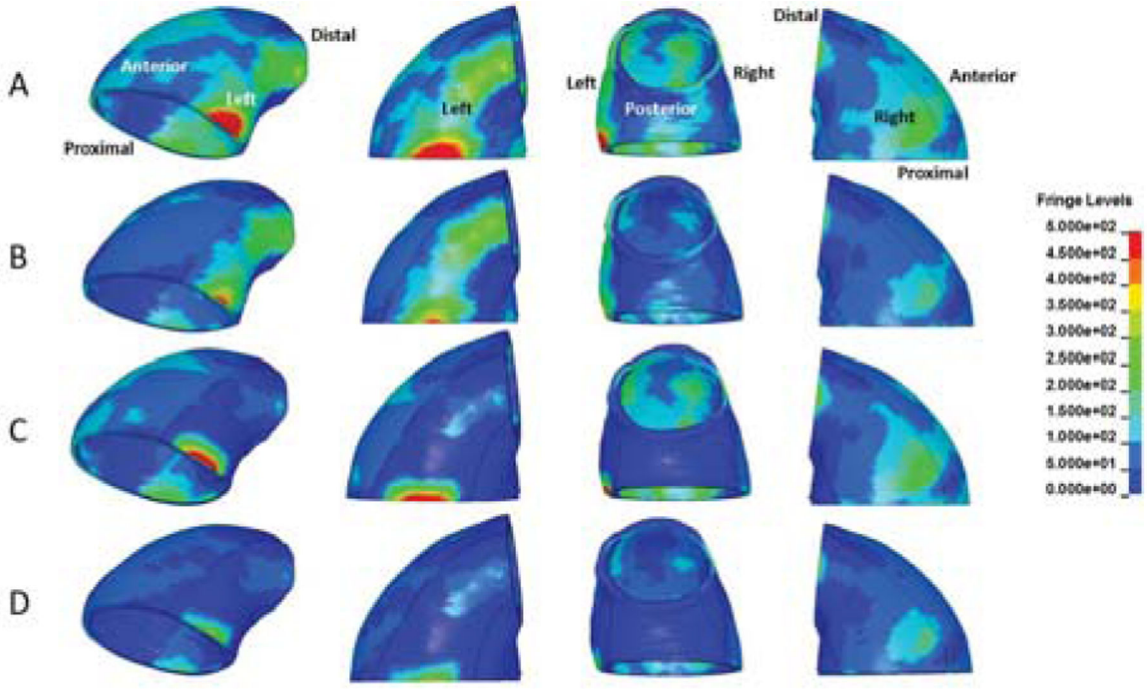

Figure 8:

Wall stress distribution of FPS and SPS at systemic pressures. Each row of figures represents four views of the same conditions: 7a) FPS at systole 7b) FPS at diastole 7c) SPS at systole 7d) SPS at diastole. Fringe levels in kPa.